Faddeev calculations of the 2π-3N force contribution to the ^{3}H binding energy

C. R. Chen* and G. L. Payne
Department of Physics and Astronomy, University of Iowa, Iowa City, Iowa 52242

J. L. Friar and B. F. Gibson
Theoretical Division, Los Alamos National Laboratory, Los Alamos, New Mexico 87545
(Received 30 December 1985)

The configuration-space Faddeev equations are solved for Hamiltonians that include the Tucson-Melbourne, Brazil, and Urbana two-pion-exchange three-nucleon force models. Convergence in terms of the number of three-body partial waves is demonstrated. First-order perturbation theory results are shown to be inadequate. All three models produce approximately 1.5 MeV additional binding, which overbinds the triton, when the standard value of the πN form factor cutoff is used.

I. INTRODUCTION

In the traditional approach of nuclear physics one describes the nucleus in terms of a model in which nonrelativistic, point nucleons interact via two-body (pairwise) forces. Subnuclear degrees of freedom are ignored. Although there is no *a priori* theoretical justification for this assumption, the simplifications inherent in the traditional model are enormous. Moreover, the consequence has been a semiphenomenological description of nuclear structure and reactions that has enjoyed considerable qualitative success. Nevertheless, the inability to calculate observables accurately for a given two-body force model has been a serious impediment to the development of a fundamental understanding of nuclear physics.

Trinucleon bound-state calculations using pairwise "realistic" potentials, potentials that reproduce the properties of the deuteron and nucleon-nucleon (NN) scattering data up to the threshold for pion production, demonstrate that such a Hamiltonian model underbinds the triton by 0.8—1.1 MeV and generates too large a charge radius by 0.1—0.2 fm.[1] This is a nontrivial test of the traditional approach; there was certainly no guarantee of success. Among the possible defects in the traditional model are the following: (1) the omission of non-negligible relativistic effects, (2) the failure to include explicitly in the NN force model meson degrees of freedom and nucleon substructure, and (3) the neglect of three-body forces, forces which depend upon the coordinates (space, spin, isospin, and possibly momenta) of three nucleons simultaneously. These three categories are, of course, not distinct and independent. However, we concentrate on the last category,[2] in part because it raises the hope of improving the agreement between the Fourier transform of the calculated ^{3}He charge density and the ^{3}He elastic electron scattering form factor.[1,3]

Because of the discrepancies between theory and experiment within the realm of the traditional model, various groups attempted to estimate the contribution of long-range three-nucleon forces to the triton binding energy.[4–9] These studies dealt primarily with the Tucson-Melbourne (TM) (Ref. 10) and Brazil (BR) (Ref. 11) two-pion-exchange (2π) models of the three-body force (3N), models which respect chiral constraints. Strong short-range repulsion of the NN force was assumed to render unimportant the short-range properties of the three-nucleon force. (An alternative approach in terms of an isobar constituent model of the Fujita-Miyazawa[12]—type was explored by Hajduk and Sauer.[13]) The diverse approximations used in estimating the three-nucleon force contribution to the triton binding energy gave the appearance of significant discrepancies among a number of the calculations.[4–9] However, the results of Refs. 8 and 9 established the numerical accuracy of the first-order perturbation theory approach. Unfortunately, they also implied a strong model dependence, which would invalidate the assumption that one need consider only the long-range part of the three-body force.

We report here details of the solution[14] of the full bound-state, configuration-space Faddeev equations to obtain exact results for the ^{3}H binding energy using the TM and BR 2π-3N models as well as the phenomenological Urbana (UR) model.[15] The salient features of the results are the following: (1) The TM model requires more than a first-order perturbative treatment to obtain even qualitatively reliable numbers; (2) all three 2π-3N models require that a large number of three-body channels (viz., 34, all two-body potential components with $j \leq 4$) be included to ensure that the answer has converged; (3) all three of the 2π-3N models lead to overbinding of ^{3}H, whether the underlying two-body Hamiltonian is based upon the stiff Reid soft-core (RSC) (Ref. 16) or the softer Argonne V14 (AV14) (Ref. 17) nucleon-nucleon force, *if* one utilizes the commonly accepted value of $\Lambda = 5.8\mu$ (μ is the pion mass) in the (monopole) π-nucleon form factor; (4) for a given value of Λ we find no significant difference in the binding energy increment arising from each model in a full calculation; and (5) unlike the situation which holds for the NN Hamiltonian alone,[18] we find that the NN odd partial waves contribute substantially to the 3N force increment in the ^{3}H binding energy, which explains why the early first-order perturbation theory calculations failed to yield valid results.

 ©1986 The American Physical Society

II. THREE-BODY FORCE MODEL

Without attempting to judge the underlying philosophies of the competing methods for constructing a three-nucleon force, we adopt for the purposes of this investigation the TM (model independent), BR (chiral Lagrangian), and UR (phenomenological) models as our ansätze. These models, have in fact, the same long-range two-pion-exchange functional form, although only the UR model includes a nonzero isoscalar term. They differ significantly in the parametrization of the short-range s-wave part of the potential. This difference should not affect the 2π-3N force contribution to the ^{3}H binding, if the short-range repulsion of the dominant NN force is strong enough to keep the nucleons apart and therefore suppress the contribution of the short-range components of the three-nucleon force.

The 2π-3N force $W(\mathbf{x}_1,\mathbf{x}_2,\mathbf{x}_3)$ can be decomposed into three parts

$$W = W_1 + W_2 + W_3 , \tag{1}$$

where the W_i each have the same functional form but contain cyclically permuted variables. Physically W_1 corresponds to the process in which particle 1 exchanges one pion with each of particles 2 and 3. The analytic expression for the TM and BR potential models is

$$\begin{aligned}
W_1 = \left[\frac{g\mu}{8M\pi}\right]^2 \Big[& (\tau_2\cdot\tau_3)(\sigma_2\cdot\hat{\mathbf{x}}_3)(-\sigma_3\cdot\hat{\mathbf{x}}_2) \\
& \times\{(a-2\mu^2 c)Z_1'(x_3)Z_1'(x_2)+c[Z_0'(x_3)Z_1'(x_2)+Z_1'(x_3)Z_0'(x_2)]\} \\
& + b(\tau_2\cdot\tau_3)\Big\{(\sigma_2\cdot\hat{\mathbf{x}}_3)(-\sigma_3\cdot\hat{\mathbf{x}}_2)(-\hat{\mathbf{x}}_3\cdot\hat{\mathbf{x}}_2)\left[Z_1''(x_3)-\frac{Z_1'(x_3)}{x_3}\right] \\
& \quad\times\left[Z_1''(x_2)-\frac{Z_1'(x_2)}{x_2}\right]+(\sigma_2\cdot\hat{\mathbf{x}}_3)(\sigma_3\cdot\hat{\mathbf{x}}_3)\left[Z_1''(x_3)-\frac{Z_1'(x_3)}{x_3}\right]\frac{Z_1'(x_2)}{x_2} \\
& \quad+(-\sigma_2\cdot\hat{\mathbf{x}}_2)(-\sigma_3\cdot\hat{\mathbf{x}}_2)\left[Z_1''(x_2)-\frac{Z_1'(x_2)}{x_2}\right]\frac{Z_1'(x_3)}{x_3} \\
& \quad+(\sigma_2\cdot\sigma_3)\frac{Z_1'(x_3)}{x_3}\frac{Z_1'(x_2)}{x_2}\Big\}+d(\tau_3\times\tau_2\cdot\tau_1) \\
& \times\Big\{(\sigma_2\cdot\hat{\mathbf{x}}_3)(-\sigma_3\cdot\hat{\mathbf{x}}_2)(-\sigma_1\cdot\hat{\mathbf{x}}_3\times\hat{\mathbf{x}}_2)\left[Z_1''(x_3)-\frac{Z_1'(x_3)}{x_3}\right]\left[Z_1''(x_2)-\frac{Z_1'(x_2)}{x_2}\right] \\
& \quad+(\sigma_2\cdot\hat{\mathbf{x}}_3)(\sigma_3\cdot\sigma_1\times\hat{\mathbf{x}}_3)\left[Z_1''(x_3)-\frac{Z_1'(x_3)}{x_3}\right]\frac{Z_1'(x_2)}{x_2} \\
& \quad+(-\sigma_3\cdot\hat{\mathbf{x}}_2)(-\sigma_1\cdot\sigma_2\times\hat{\mathbf{x}}_2)\left[Z_1''(x_2)-\frac{Z_1'(x_2)}{x_2}\right]\frac{Z_1'(x_3)}{x_3} \\
& \quad+(\sigma_1\cdot\sigma_2\times\sigma_3)\frac{Z_1'(x_3)}{x_3}\frac{Z_1'(x_2)}{x_2}\Big\}\Big] ,
\end{aligned} \tag{2}$$

where we use the relative coordinate definition $\mathbf{x}_i=\mathbf{r}_j-\mathbf{r}_k$. Here $g^2=179.7$ is the coupling constant, $\mu=139.6$ MeV and $M=6.726\mu$ are the pion and nucleon masses, and σ_i and τ_i are the spin and isospin operators that act on particle i. The remaining functions are

$$Z_0'(r)=-\frac{(\Lambda^2-\mu^2)^2}{2\mu}e^{-\Lambda r}, \tag{3a}$$

$$Z_1'(r)=-\mu\left[1+\frac{1}{\mu r}\right]\frac{e^{-\mu r}}{\mu r}+\Lambda\left[1+\frac{1}{\Lambda r}\right]\frac{e^{-\Lambda r}}{\mu r}+\frac{(\Lambda^2-\mu^2)}{2\mu}e^{-\Lambda r}, \tag{3b}$$

$$Z_1''(r)-\frac{Z_1'(r)}{r}=\mu^2\left[\left[1+\frac{3}{\mu r}+\frac{3}{\mu^2 r^2}\right]\frac{e^{-\mu r}}{\mu r}-\frac{\Lambda^2}{\mu^2}\left[1+\frac{3}{\Lambda r}+\frac{3}{\Lambda^2 r^2}\right]\frac{e^{-\Lambda r}}{\mu r}-\frac{1}{2}\frac{\Lambda}{\mu}\left[\frac{\Lambda^2}{\mu^2}-1\right]\left[1+\frac{1}{\Lambda r}\right]e^{-\Lambda r}\right] . \tag{3c}$$

The πN form-factor cutoff Λ is the critical parameter in the calculation; we look at three values below. The actual form of W_1 used in our calculations was reexpressed in terms of irreducible tensor operators. Although very useful, this form does not lead to further insight and will not be displayed here. It can be found in Appendix F of Ref. 19. One final comment to be made is the following: Note that because $\mathbf{x}_2 \equiv \mathbf{x}_{31}$, in contrast to the definition of Coon and Glöckle[10] (where $\mathbf{x}_2 = -\mathbf{x}_{31}$), there are sign differences in Eq. (2) compared to the expression of Ref. 10. Thus, we begin this discussion with the expression from Ref. 15.

The UR model differs from the form shown in Eqs. (2) and (3) in that it includes an additional isoscalar term as well as a Gaussian cutoff.[15] We include it in this study because it is in contemporary use for binding energy and momentum distribution calculations for three-body and four-body nuclei and the properties of nuclear matter.

The TM and BR model parameters are specified in Table I. The c term is the singular (δ-functionlike) part of the potential. For the BR model, one has $c=0$, which means that it is much less singular than the TM model. This is borne out by the numerical results in Sec. IV, which show that the perturbation series for the TM model converges much more slowly than that for the BR model. A similar analysis holds for the UR model. We emphasize that our purpose is not to argue the validity of any one model but to produce benchmark calculations, which can be used to determine the best means of exploring three-body force effects.

TABLE I. Two-pion-exchange three-nucleon force parameters for the TM and BR models.

	μa	$\mu^3 b$	$\mu^3 c$	$\mu^3 d$
TM	1.130	−2.580	1.00	−0.7530
BR	1.048	−2.287	0.0	−0.7656

III. NUMERICAL METHODS

Following the procedures used in our previous configuration-space Faddeev calculations,[20] we decompose the total wave function for three identical nucleons into a sum of three Faddeev[21] amplitudes:

$$\Psi = \psi(\mathbf{x}_1,\mathbf{y}_1)+\psi(\mathbf{x}_2,\mathbf{y}_2)+\psi(\mathbf{x}_3,\mathbf{y}_3) \equiv \psi_1+\psi_2+\psi_3 \,. \tag{4}$$

We use the Jacobi coordinates

$$\mathbf{x}_i = \mathbf{r}_j - \mathbf{r}_k \,, \tag{5a}$$

$$\mathbf{y}_i = \tfrac{1}{2}(\mathbf{r}_j+\mathbf{r}_k) - \mathbf{r}_i \,, \tag{5b}$$

where i, j, and k denote cyclic permutation.

The Hamiltonian for the system is of the form

$$H = T + \sum_i V(\mathbf{x}_i) + W(\mathbf{x}_1,\mathbf{x}_2,\mathbf{x}_3) \,, \tag{6}$$

where W is the 2π-3N force defined in Sec. II. There are many ways to decompose the Schrödinger equation into coupled Faddeev equations in the presence of a three-body force. Three possible choices are

$$[T+V(\mathbf{x}_i)-E]\psi_i = -V(\mathbf{x}_i)(\psi_j+\psi_k) - W_i\Psi \,, \tag{7a}$$

$$[T+V(\mathbf{x}_i)-E]\psi_i = -V(\mathbf{x}_i)(\psi_j+\psi_k) - W\Psi_i \,, \tag{7b}$$

$$[T+V(\mathbf{x}_i)-E]\psi_i = -V(\mathbf{x}_i)(\psi_j+\psi_k) - \tfrac{1}{3}W\Psi \,. \tag{7c}$$

For identical particles the amplitudes ψ_i ($i=1,2,3$) all have the same functional form, so that it is only necessary to solve one of the Faddeev equations and cyclically permute the variables to obtain the remaining amplitudes required to construct the Schrödinger wave function corresponding to Eq. (4). In each of the decompositions specified in Eq. (7), the three-body force is retained on the right-hand side of the equation. Thus, the NN tensor force couples at most two channels on the left-hand side, which is convenient for the numerical solution of the equations. Finally, each of the Faddeev equation decompositions must lead to the same binding energy when we include all (or a sufficient number of) partial waves. However, we shall see below that in practice the methods do not exhibit the same rate of convergence.

We use the j-J coupling scheme in our partial wave representation of the Faddeev amplitudes. The ψ_i is written in the form:

$$\psi(\mathbf{x}_i,\mathbf{y}_i) = \sum_\alpha \frac{\psi_\alpha(x_i,y_i)}{x_i y_i} \,|\, [(l_\alpha,s_\alpha)j_\alpha;(L_\alpha,S_\alpha)J_\alpha]\mathcal{J}M;(t_\alpha,T_\alpha)\mathcal{T}M_T\rangle_i \,,$$
$$= \sum_\alpha \frac{\psi_\alpha(x_i,y_i)}{x_i y_i} \,|\, \alpha\rangle_i \,, \tag{8}$$

where l_α is the orbital angular momentum of particles j and k, s_α is the spin angular momentum of particles j and k, j_α is the total angular momentum of particles j and k, L_α is the orbital angular momentum of particle i relative to the center of mass of particles j and k, S_α is the spin of particle i ($S_\alpha=\frac{1}{2}$), J_α is the total angular momentum of particle i, $\mathcal{J}$ is the total angular momentum of the three-particle system, t_α is the total isospin of particles j and k, T_α is the isospin of particle i ($T_\alpha=\frac{1}{2}$), and $\mathcal{T}$ is the total isospin of the three-particle system.

To obtain the partial-wave projections of Eqs. (7a)–(7c), we multiply by $x_i y_i$ and form the inner product with ${}_i\langle\alpha|$. In addition, following Noyes,[22] we introduce the hyperspherical variables

$$x_1 = \rho\cos\theta \tag{9a}$$

and

$$y_1=\tfrac{1}{2}\sqrt{3}\rho\sin\theta, \tag{9b}$$

as well as the cosine of the angle between $\mathbf{x}_1$ and $\mathbf{y}_1$

$$\mu=\frac{\mathbf{x}_1\cdot\mathbf{y}_1}{x_1y_1}. \tag{9c}$$

This change of variables simplifies the projection integrals on the right-hand side of the equation, as they depend only upon the single variable θ and not ρ. Equation (7a) can then be written in the form

$$(\Delta_\alpha-\kappa^2)\psi_\alpha(\rho,\theta)-\sum_\beta v_{\alpha\beta}(\rho\cos\theta)\psi_\beta(\rho,\theta)=\sum_{\beta\gamma}[v_{\alpha\beta}(\rho\cos\theta)+w^1_{\alpha\beta}(\rho,\theta,\mu)]\int_{\theta^-}^{\theta^+}K_{\beta\gamma}(\theta,\theta')\psi_\gamma(\rho,\theta')d\theta'+\sum_\beta w^1_{\alpha\beta}\psi_\beta(\rho,\theta), \tag{10}$$

where $\kappa^2=-ME/\hbar^2$ and we define

$$\Delta_\alpha=\frac{\partial^2}{\partial\rho^2}+\frac{1}{\rho}\frac{\partial}{\partial\rho}+\frac{1}{\rho^2}\frac{\partial^2}{\partial\theta^2}-\frac{l_\alpha(l_\alpha+1)}{\rho^2\cos^2\theta}-\frac{L_\alpha(L_\alpha+1)}{\rho^2\sin^2\theta}, \tag{11}$$

$$v_{\alpha\beta}(\rho\cos\theta)=\frac{M}{\hbar^2}{}_1\langle\alpha\,|\,V(\mathbf{x}_1)\,|\,\beta\rangle_1, \tag{12}$$

$$w^1_{\alpha\beta}(\rho,\theta,\mu)=\frac{M}{\hbar^2}{}_1\langle\alpha\,|\,W_1(\mathbf{x}_1,\mathbf{x}_2,\mathbf{x}_3)\,|\,\beta\rangle_1. \tag{13}$$

[Note that we have used the relationship

$${}_1\left\langle\alpha\left|\frac{\psi_\beta(x_2,y_2)}{x_2y_2}\right|\beta\right\rangle_2={}_1\left\langle\alpha\left|\frac{\psi_\beta(x_3,y_3)}{x_3y_3}\right|\beta\right\rangle_3$$

to simplify Eq. (10).] The kernels $K_{\beta\gamma}(\theta,\theta')$ can be evaluated by means of standard angular momentum recoupling techniques.[23] The θ^+ and θ^- limits for the $K_{\beta\gamma}$ projection integral are defined in Ref. 20. The partial wave equations which correspond to Eqs. (7b) and (7c) are basically the same as Eq. (10), differing only in the projection of the 3N force term. We, therefore, illustrate the calculational method only for the decomposition defined by Eq. (7a).

Numerical solution of the partial wave equations is facilitated by defining a smoother function $F_\alpha(\rho,\theta)$, which has the asymptotic part of the $\psi_\alpha(\rho,\theta)$ amplitude factored out. Using the definition

$$\psi_\alpha(\rho,\theta)=F_\alpha(\rho,\theta)\frac{e^{-\kappa\rho}}{\rho^{1/2}}, \tag{14}$$

we can rewrite Eq. (10) as

$$\left[\frac{\partial^2}{\partial\rho^2}+\frac{1}{4\rho^2}+\frac{1}{\rho^2}\frac{\partial^2}{\partial\theta^2}-2\kappa\frac{\partial}{\partial\rho}-\frac{l_\alpha(l_\alpha+1)}{\rho^2\cos^2\theta}-\frac{L_\alpha(L_\alpha+1)}{\rho^2\sin^2\theta}\right]F_\alpha(\rho,\theta)-\sum_\beta v_{\alpha\beta}(\rho\cos\theta)F_\beta(\rho,\theta)$$
$$=\sum_{\beta\gamma}(v_{\alpha\beta}+w^1_{\alpha\beta})\int_{\theta^-}^{\theta^+}K_{\beta\gamma}(\theta,\theta')F_\gamma(\rho,\theta')d\theta'+\sum_\beta w^1_{\alpha\beta}F_\beta(\rho,\theta). \tag{15}$$

The boundary conditions for $F_\alpha(\rho,\theta)$ are

$$F_\alpha(\rho,\theta)=0 \text{ for } \rho=0, \tag{16a}$$

$$F_\alpha(\rho,\theta)=0 \text{ for } \theta=0 \text{ and } \theta=\pi/2, \tag{16b}$$

$$\frac{\partial F_\alpha(\rho,\theta)}{\partial\rho}=0 \text{ for } \rho=\rho_{\max}. \tag{16c}$$

These boundary conditions are easily implemented. However, Eq. (16c) is not exact for $\theta\simeq\pi/2$.[24] Nevertheless, for the bound-state problem, the error in the wave function due to the use of this approximate boundary condition is negligible, because the wave function is negligibly small for sufficiently large $\rho_{\max}$.

To solve Eq. (15), we use the method of orthogonal collocation.[25] First, the $F_\alpha(\rho,\theta)$ functions are expanded in bicubic Hermite splines on a rectangular grid in ρ-θ coordinates:

$$F_\alpha(\rho,\theta)=\sum_{m=1}^{M}\sum_{n=1}^{N}a^\alpha_{mn}s_m(\rho)s_n(\theta). \tag{17}$$

The boundary conditions are easy to impose for this expansion; they translate into a requirement that the expansion coefficients a^α_{mn} for some of the splines be zero. Second, the collocation procedure then demands that the values of the remaining a^α_{mn} be determined by the requirement that the $F_\alpha(\rho,\theta)$ satisfy Eq. (15) at the M distinct values of ρ_i and the N distinct values of θ_j, which are the collocation points. If one selects these points to be the two-point Gauss-Legendre quadrature points for each interval, then the procedure is known as orthogonal collocation.

Our resulting equation is

$$\sum_{m=1}^{M}\sum_{n=1}^{N}\left\{s_m''(\rho_i)s_n(\theta_j)+\frac{1}{\rho_i^2}\left[\frac{1}{4}-\frac{l_\alpha(l_\alpha+1)}{\cos^2\theta_j}-\frac{L_\alpha(L_\alpha+1)}{\sin^2\theta_j}\right]s_m(\rho_i)s_n(\theta_j)+\frac{1}{\rho_i^2}s_m(\rho_i)s_n''(\theta_j)\right.$$
$$\left.-2\kappa s_m'(\rho_i)s_n(\theta_j)\right\}a_{mn}^{\alpha}-\sum_{m=1}^{M}\sum_{n=1}^{N}\sum_{\beta}v_{\alpha\beta}(\rho_i\cos\theta_j)s_m(\rho_i)s_n(\theta_j)a_{mn}^{\beta}$$
$$=\sum_{m=1}^{M}\sum_{n=1}^{N}\sum_{\gamma}\left\{\sum_{\beta}(v_{\alpha\beta}+w_{\alpha\beta}^{1})\int_{\theta^-}^{\theta^+}K_{\beta\gamma}(\theta_j,\theta')s_m(\rho_i)s_n(\theta')d\theta'\right\}a_{mn}^{\gamma}+\sum_{m=1}^{M}\sum_{n=1}^{N}\sum_{\beta}w_{\alpha\beta}^{1}s_m(\rho_i)s_n(\theta_j)a_{mn}^{\beta}\ . \quad (18)$$

This is a matrix equation of the form

$$Aa=Ba\ , \quad (19)$$

where A depends parametrically upon the eigenvalue κ. Following the procedures described in detail in Ref. 26, we introduce the parameter λ and rewrite Eq. (19) as

$$Aa=\lambda Ba\ . \quad (20)$$

To determine the energy of the bound state, we search for a value of κ for which Eq. (20) has a solution such that the linear eigenvalue λ is unity. Because we retain the three-body force terms on the right-hand side of Eq. (18), we preserve the numerical advantage described in detail in Ref. 26, and we can use that same variation of the power method to solve the eigenvalue equation iteratively for smaller numbers of channels. However, the Lanczos method[27] as generalized by Saad[28] for nonsymmetric systems, which is the case for the Hamiltonian of the Faddeev equations we are solving, provides even faster convergence. (See the Appendix.) It was this procedure that we used to solve the large 34-channel problem.

In order to check our eigenvalue solutions, we use the wave functions which we generate to calculate variational upper bounds:[29]

$$\langle H\rangle=\langle\Psi|H|\Psi\rangle/\langle\Psi|\Psi\rangle$$
$$=\langle\Psi|T+V+W|\Psi\rangle/\langle\Psi|\Psi\rangle\ , \quad (21)$$

where $V=\sum V(\mathbf{x}_i)$. The NN potential V is always assumed to act only in a given number of NN partial waves. By projecting W_1 (or $\frac{1}{3}W$) in the same manner as V, we obtain a test of the accuracy of our eigenvalue solution; symbolically we have

$$\langle H_P\rangle=\langle\Psi|P\rangle\langle P|T+V+W|P\rangle\langle P|\Psi\rangle/\langle\Psi|\Psi\rangle\ . \quad (22)$$

When we do not use a projected three-body force, we obtain a variational upper bound on the projected two-body plus full three-body Hamiltonian:

$$H=(T+V)_P+W\ . \quad (23)$$

By comparing $\langle H_P\rangle$ and E_F for Eqs. (7a) or (7c), we can estimate the quality of the wave function; this procedure is not valid for Eq. (7b). By comparing $\langle H\rangle$ with E_F, we can investigate how the calculation is converging. When a sufficient number of partial waves have been included, then $\langle H_P\rangle$ and $\langle H\rangle$ will have the same value.

IV. NUMERICAL RESULTS

In order to interpret the three-body force results which we have obtained, we first recall the binding energies and charge radii of the RSC and AV14 nucleon-nucleon potential models for 5, 9, 18, and 34 channels.[26] (See Table II.) The number of three-body channels is directly related to $j_{\max}$ and the parity of the NN-force partial waves retained for the calculation:

5 channel $\sim j\le 1,+$,

9 channel $\sim j\le 2,+$,

18 channel $\sim j\le 2,\pm$,

34 channel $\sim j\le 4,\pm$.

TABLE II. Binding energies and point nucleon charge radii for the RSC and AV14 potential models as a function of the number of channels.

		$-E_0$ (MeV)	$\langle r^2\rangle_{\rm ch}^{1/2}(^3\mathrm{He})$ (fm)	$\langle r^2\rangle_{\rm ch}^{1/2}(^3\mathrm{H})$ (fm)
RSC	5	7.02	1.89	1.70
	9	7.21	1.87	1.68
	18	7.23	1.87	1.58
	34	7.35	1.85	1.67
AV14	5	7.44	1.86	1.68
	9	7.57	1.84	1.67
	18	7.57	1.84	1.67
	34	7.67	1.83	1.67
Expt.		8.48	1.74(3)	1.61(4)

The stiff RSC potential model (stronger short-range repulsion) calculation converges more slowly than that for the softer AV14 potential model. The odd partial waves (compare 18 channels with 9 channels) contribute little to the ^{3}H energy. The increase in binding between 18 channels and 34 channels was shown in Ref. 26 to come almost entirely from the additional even-parity NN potential partial waves. We believe the contribution to the binding energy of NN partial waves with $j>4$ to be only a few keV. The radii decrease as expected with the increase in binding energy as the number of channels in the calculation is increased. (A comparison of these results with those of other groups and with other potential models can be found in Ref. 15.)

Numerical solution for both Ψ_0 (no three-body force) and for Ψ (two-body plus three-body force) was achieved in terms of the spline expansion procedure outlined above. The ρ and θ breakpoints were distributed differently. The ρ breakpoint distribution was scaled according to $\rho_{n+1}-\rho_n=(\rho_n-\rho_{n-1})S_\rho$, where S_ρ is the scale factor. The θ breakpoints were distributed uniformly in each of three equally spaced intervals between 0 and $\pi/2$. The largest number of breakpoints were placed in the interval nearest $\pi/2$, where the NN potential is strongest. For most calculations we used 14 ρ breakpoints scaled by $S_\rho=1.3$ with $\rho_{\max}=16$ or 20 fm. The θ distribution was (9,3,2). The strength parameter λ was solved for as a function of κ, and an extrapolation to $\lambda=1$ was made to determine the binding energy. To test our numerical accuracy, we also performed calculations with as many as 20 ρ and θ breakpoints; this led to differences in the triton binding energy of less than 10 keV.

In Table III we display the eigenvalue and expection values obtained with each of the three procedures (W_1, W, and $\frac{1}{3}W$) defined in Eqs. (7a)—(7c) as a function of the number of three-body channels for the model comprised of the RSC NN force and the BR 3N force (RSC/BR). (Clearly $E_F=\langle H_P\rangle$ to a good approximation for the W_1 and $\frac{1}{3}W$ prescriptions, where the procedure is applicable.) Table IV exhibits similar results for the AV14/TM model. (Note that differences between these results and those quoted in Ref. 14 are due to a better extrapolation to $\lambda=1$.) Because these results establish that the calculations converge for 34 channels, we did not run the full set of calculations for each procedure in the case of RSC/TM and AV14/BR models.

The results for the RSC/BR model (Table III) clearly indicate that 34 channels are required to obtain a valid estimate of the ^{3}H binding energy, when such a three-body force is included in the Hamiltonian. Full agreement between E_F (and therefore $\langle H_P\rangle$) and $\langle H\rangle$ is not obtained for fewer than 34 channels, whereas all three procedures arrive at approximately the same value of E_F and $\langle H\rangle$ when 34 channels are included. Clearly the odd parity NN partial waves play a significant role when a three-body force is present, because E_F (and $\langle H\rangle$) changes considerably in going from 9 to 18 to 34 channels. Comparison of the $\langle T+V_P\rangle$ expectation using Ψ with the corresponding NN potential model eigenvalues in Table II shows that Ψ contains much more structure (at short distances where W is largest) than Ψ_0 from the two-body Hamiltonian. (The kinetic energy expectation increases as the structure in the wave function grows.) The 2π-3N force pushes the wave function out of the region of the origin. However, the increased binding pulls in the exterior part of Ψ, as the exponential tail must fall off faster. The result is an enhancement of the peak of Ψ corresponding to the equilateral configuration compared to the peak corresponding to the colinear configuration. The effect of this upon the ^{3}He charge density will be discussed elsewhere.

Based upon the results of Table III, it is difficult to say which Faddeev equation decomposition of the three-body force is to be preferred. Such is not the case for the AV14/TM model whose results are shown in Table IV. Here the results are incomplete for the W prescription, because for 18 channels (the first chance to include negative-parity NN-potential waves), the eigenvalue was several hundred MeV. If a sufficient number of three-body channels had been included, then the correct result

TABLE III. Triton binding energies (in MeV) for the RSC/BR model as a function of the number of three-body channels for the three Faddeev equation decomposition defined by Eqs. (7a)—(7c). Subscript P denotes the appropriate projection as discussed in the text.

	No. of channels	$-E_F$	$-\langle H_P\rangle$	$-\langle W_P\rangle$	$-\langle W\rangle$	$-\langle H\rangle$
W_1	5	7.66	7.66	0.81	1.43	8.28
	9	8.77	8.77	2.11	1.94	8.60
	18	8.71	8.70	1.90	1.93	8.72
	34	8.89	8.89	1.98	2.00	8.91
W	5	7.64			1.35	8.26
	9	8.32			1.65	8.61
	18	8.77			1.91	8.71
	34	8.91			2.00	8.90
$\frac{1}{3}W$	5	7.38	7.38	0.42	1.32	8.28
	9	7.99	7.99	0.94	1.60	8.64
	18	8.55	8.54	1.66	1.83	8.71
	34	8.89	8.89	1.98	2.00	8.91

TABLE IV. Triton binding energies (in MeV) from the AV14/TM model as a function of the number of three-body channels for the three Faddeev decompositions defined by Eqs. (7a)–(7c). Subscript P denotes the appropriate projection as discussed in the text.

	No. of channels	$-E_F$	$-\langle H_P\rangle$	$-\langle W_P\rangle$	$-\langle W\rangle$	$-\langle H\rangle$
W_1	5	8.26	8.26	1.98	1.93	8.22
	9	8.96	8.96	2.77	2.22	8.40
	18	9.49	9.50	3.29	2.88	9.08
	34	9.36	9.36	2.88	2.84	9.32
W	5	8.12			1.40	8.31
	9	8.64			1.61	8.48
	18					
	34					
$\frac{1}{3}W$	5	7.82	7.82	0.69	1.23	8.36
	9	8.34	8.35	1.23	1.44	8.57
	18	9.10	9.11	2.61	2.61	9.11
	34	9.33	9.33	2.85	2.84	9.32

would have emerged. But this anomalous result for 18 channels caused us to reject this procedure for the TM force calculations and not to complete Table IV. The 18-channel eigenvalue for the W_1 procedure also overshoots the result for the full calculation. This peculiar behavior probably accounts for the remaining lack of convergence apparent in the 34-channel eigenvalue. Otherwise, the comments made above for the RSC/BR model hold also for the AV14/TM model.

The convergence of the solution for the less singular BR 3N-force model is obviously faster than for the TM model. This is made quantitative in Table V. There we compile the results of Hajduk's perturbation series[26,30,33] for $E=\langle\Psi|H|\Psi\rangle$ (for both models using the W_1 prescription to generate Ψ)

$$\langle\Psi|H|\Psi\rangle=E_0+E_1+E_2+E_3\ .$$

We have defined:

$$E_0=\langle\Psi_0|H_{\rm NN}|\Psi_0\rangle\ ,$$
$$E_1=\langle\Psi_0|W|\Psi_0\rangle\ ,$$
$$E_2=3(E-E_0)-2E_1-\overline{\Delta E}\ ,$$
$$E_3=-2(E-E_0)+E_1+\overline{\Delta E}\ ,$$
$$\overline{\Delta E}=\langle\Psi|W|\Psi\rangle\ ,$$

where $H_{\rm NN}=T+V$ is the NN-force Hamiltonian, Ψ_0 is its eigenfunction, and one *assumes* that $E_i=0$ for $i\geq 4$. Obviously this series can be generated only because we have solved for the complete solution Ψ. However, comparing E_1, E_2, and E_3 permits one to understand how well perturbation theory works. It is clear from Table V that for the RSC/BR model the first-order E_1 result is the dominant part of the $E-E_0$ difference. However, for the AV14/TM model there is clearly no convergence. We do not find $E_1\gg E_2\gg E_3$. Furthermore, E_1 as a function of the number of channels varies significantly. Finally, the strong model dependence of the five-channel result as well as the small value of E_1 (for the TM force) accounts for most of the disparate results found in the literature.[4–9] This failure of the first-order perturbation-theory estimate for $\langle\Psi_0|W|\Psi_0\rangle$ can be seen by comparing results of Refs. 8 and 9 with ours. Wiringa *et al.*[8] obtained $\langle H_{\rm NN}\rangle=-7.29$ MeV and $\langle W\rangle=-0.14$ MeV for the AV14/TM model in the five-channel approximation. (Here $\langle W\rangle$ is the full, unprojected three-body force.) Ishikawa *et al.*[9] agreed with the Wiringa *et al.* estimate for the five-channel calculation and made the first RSC/TM 18-channel estimate obtaining $\langle H_{\rm NN}\rangle=-7.22$ MeV and $\langle W\rangle=-0.89$ MeV. Our calculations agree completely with those results for first-order perturbation theory using the unprojected three-body force. However, the -0.14 MeV is far from our 34-channel value of $E-E_0=-1.69$ MeV for the AV14/TM model and the -0.89 MeV is far from our 34-channel value of $E-E_0=-1.53$ MeV for the RSC/TM model. First-order perturbation theory is simply inadequate for es-

TABLE V. Perturbation series energies (in MeV) as a function of the number of three-body channels for the AV14/TM and RSC/BR models using the W_1 Faddeev equation decomposition.

	No. of channels			
	5	9	18	34
		AV14/TM		
$-E$	8.26	8.96	9.50	9.36
$-E_0$	7.44	7.57	7.57	7.67
$-E_1$	−0.13	0.35	0.92	0.76
$-E_2$	0.76	0.71	0.66	0.63
$-E_3$	0.20	0.34	0.35	0.29
		RSC/BR		
$-E$	7.64	8.76	8.69	8.89
$-E_0$	7.02	7.21	7.23	7.34
$-E_1$	0.49	1.13	1.10	1.17
$-E_2$	0.09	0.30	0.27	0.31
$-E_3$	0.05	0.13	0.08	0.06

timating three-nucleon force effects in the triton, because second-order modifications of the wave function (in particular, the odd partial waves) are large.

In Table VI we summarize the triton binding energy results for all six combinations of the three-body force models (TM, BR, UR) with the NN force models (RSC, AV14) which we have studied. First, note that the 0.4 (0.3) MeV difference between the AV14/TM (AV14/BR) and RSC/TM (RSC/BR) binding energies is essentially the same difference that is seen in Table II when one compares the triton binding energies of the AV14 and RSC NN force models in the absence of a three-body force. The same holds for the 0.3 MeV difference between the AV14/UR and RSC/UR binding energies. Second, each of these three-nucleon force models yields approximately the same 1.5 additional binding energy for the triton. The slightly smaller binding energy increase in the case of the UR model ($\sim$0.2 MeV) is likely a reflection of the different form of the πN form factor cutoff in that model; we discuss below the sensitivity to Λ in the case of the TM model. Third, the RSC 34-channel eigenvalues for the TM and BR models are very similar; the strong short-range repulsion of the RSC NN force does effectively suppress the contribution of the more singular TM 2π-3N force model. The softer AV14 NN force does allow small differences in the 2π-3N force models to be seen.

Each of these three-body force models provides too much additional binding. However, these three-nucleon force models neglect the $\rho\pi$ and heavier meson contributions to the 3N force.[31] The choice of $\Lambda=5.8\mu$ (the value consistent with the current view that one-half the Goldberger-Trieman discrepancy is attributable to form-factor effects[32]) as the πN form factor cutoff appears to be much more critical. We quote in Table VII results for the ^{3}H binding energy using the RSC/TM model for three values of Λ. There obviously exists a value of Λ for which the theoretical binding energy matches the experimental value for the triton. However, again we emphasize that our purpose is not to claim a valid model calculation of the triton binding energy, but rather to produce benchmark calculations which can be used to explore three-body force effects. Modeling the three-nucleon force is in its infancy. We hope that these calculations will stimulate further work in this area.

TABLE VI. The 5-channel, 9-channel, 18-channel, and 34-channel triton binding energies (negative of the W_1 eigenvalues in MeV) for six model combinations.

	No. of channels			
	5	9	18	34
Model				
AV14/TM	8.26	8.94	9.49	9.36
AV14/BR	8.32	9.27	9.06	9.22
AV14/UR	7.70	8.34	8.77	8.99
RSC/TM	7.54	8.33	8.93	8.86
RSC/BR	7.66	8.77	8.71	8.89
RSC/UR	7.22	8.00	8.43	8.70

TABLE VII. Triton binding energies (in MeV) for the RSC/TM model using the W_1 Faddeev equation decomposition with various values of the πN factor cutoff Λ.

No. of channels	$\Lambda=4.1\mu$	$\Lambda=5.8\mu$	$\Lambda=7.1\mu$
5	6.93	7.55	8.75
9	7.27	8.33	10.30
18	7.44	8.93	11.40
34	7.46	8.86	11.16

In Table II we quote values of the ^{3}He and ^{3}H point-nucleon charge radii. As noted above, they decrease as the binding energy increases. (We have not included the proton-proton Coulomb repulsion in these numbers; such an effect has been shown[33] to increase the ^{3}He radius by less than 0.03 fm.) We have computed ^{3}He and ^{3}H charge radii with our 3N-force wave functions. We find that the radii are too small when ^{3}H is overbound. In Fig. 1 we plot a collection of model ^{3}He and ^{3}H radii values along with least square fitted curves. The curves agree well with the datum for each nucleus.[34] Thus, a model which yields the correct ^{3}H and ^{3}He binding should produce correct rms radii. Separating the radii into isoscalar and difference values also shows that the agreement between theory and experiment is very good.[35] (See Fig. 2.)

We have also calculated the point Coulomb energy of ^{3}He in the presence of the 2π-3N force. For the RSC/TM model we obtain a ^{3}He-^{3}H eigenvalue difference of 0.64 MeV, in complete agreement with the perturbation theory estimate. This is quite consistent with the reduction in size of ^{3}He and ^{3}H due to the increase in binding energies arising from the inclusion of the 2π-3N force.[35]

Our results for the UR model differ from those of the variational calculation of Schiavilla *et al.*[15] They report a value of -8.37 ± 0.1 MeV for the triton binding energy in the AV14/UR model. We obtain -9.0 MeV or some 0.6 MeV more binding. This difference is likely due in part to the large contribution of the odd parity NN partial waves in our solution. However, there is a 0.4 MeV difference in the ^{3}H binding energy calculated by the two methods for just the AV14 NN force alone: the variational method yields[36] -7.30 ± 0.07 MeV compared with our -7.67 MeV from the Faddeev procedure. There is a small disagreement with Sasakawa's group concerning the results for the TM and BR 2π-3N models combined with either the RSC or AV14 NN potential.[37] In this case the reason for the difference is not understood, as we do agree on the results for the NN force calculation alone.

V. CONCLUSIONS

We have solved the configuration-space Faddeev equations to obtain "exact" results for the ^{3}H binding energy using the Tuscson-Melbourne, Brazil, and Urbana two-pion-exchange three-nucleon force models (in combination with the realistic phenomenological Reid soft-core and Argonne AV14 nucleon-nucleon potentials). The TM model requires more than a first-order perturbation theory

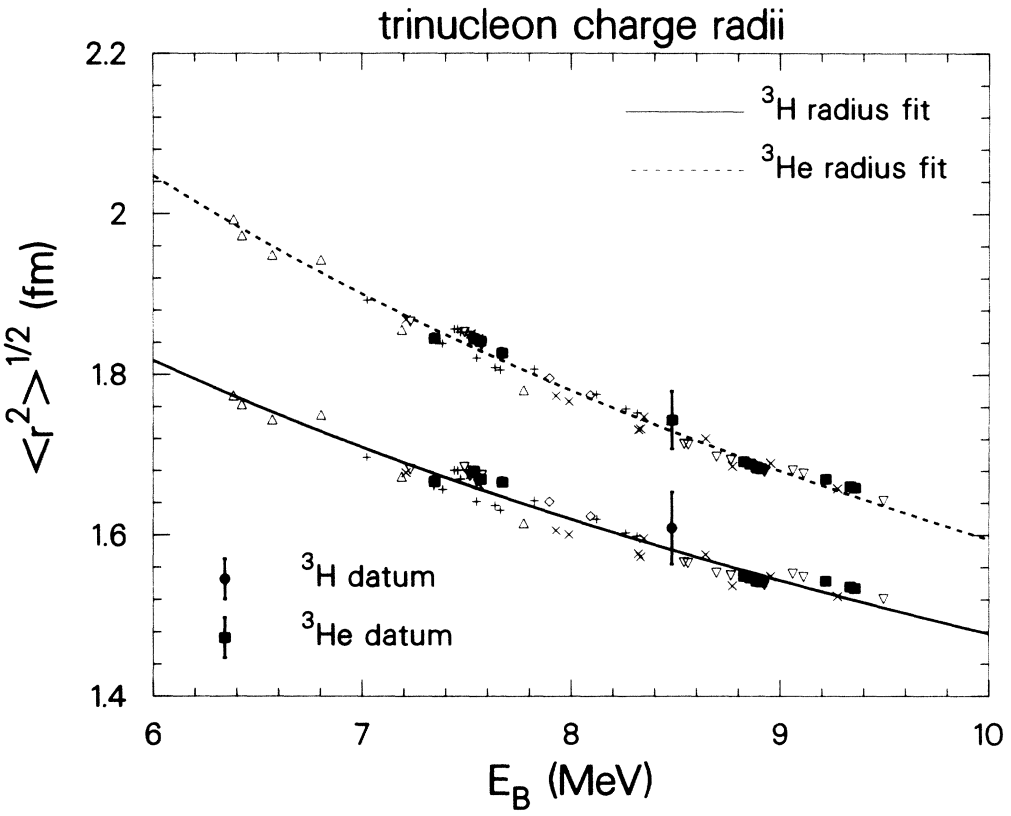

FIG. 1. The ^{3}H and ^{3}He rms point charge radii plotted vs E_B, the triton binding energy, for various model Hamiltonians. The symbols refer to the number of three-body channels in the calculation; individual entries can be found in Refs. 18 and 19. The data are from Frois (Ref. 34).

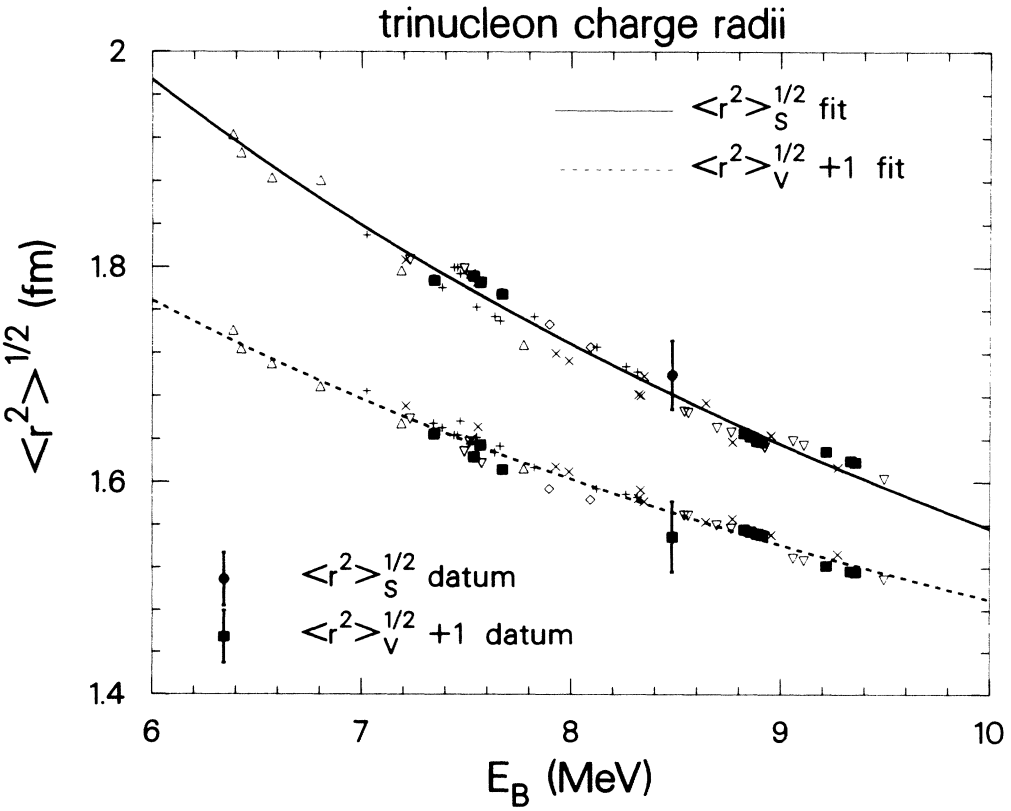

FIG. 2. The rms isoscalar and vector (difference) point charge radii plotted vs E_B, the triton binding energy, for various model Hamiltonians. The symbols refer to the number of three-body channels in the calculation; individual entries can be found in Refs. 18 and 19. The data are from Frois (Ref. 34).

treatment to obtain even qualitatively correct results. All 2π-3N models require at least 34 three-body channels to ensure that the answer has converged, which means including all NN partial waves with $j \leq 4$. Unlike the situation in the case of the NN force alone, the inclusion of these 2π-3N forces leads to large contributions from the NN odd partial waves, which explains why first-order perturbation theory calculations fail. For a given value of Λ in the monopole πN form factor, each of the 2π-3N models leads to approximately the same increase in binding. If one uses the commonly accepted value ($\Lambda = 5.8\mu$), then each of the models overbinds the triton by about 1.5 MeV. The stronger repulsion of the RSC NN force tends to mask the differences that exist between the TM and BR models in the parametrization of the short-range s-wave part of the three-nucleon force. The convergence of the binding energy calculation is no worse for the UR model with its additional isoscalar repulsive term than for the TM and BR models. However, the use of the Gaussian cutoff in the UR model makes an exact comparison between it and the TM and BR models difficult to make. Still, all three models yield essentially the same result in a complete calculation of 34 three-body channels.

Furthermore, we confirm that the low energy properties of the ^{3}H and ^{3}He system appear to scale with energy independently of the mechanism (enhanced NN singlet force, three-body force, etc.) used to modify the trinucleon binding.[35] The rms radii and the Coulomb energy are two such examples. If one obtains the correct binding energy, then agreement with the experimental radii is obtained. The Coulomb energy is exactly what one expects from perturbation theory, again being determined by the size of the system as reflected in the binding.

Note added in proof. Prof. Robilotta has pointed out that a more correct interpretation of the BR model would lead to $a \approx -1.048$ instead of the $+1.048$ quoted in Table I. Such a value of a results in an eigenvalue in the RSC/BR model of $E_F = -9.09$ MeV instead of -8.89 MeV.

ACKNOWLEDGMENTS

The work of C.R.C. and G.L.P. was supported in part by the U.S. Department of Energy. The work of J.L.F. and B.F.G. was performed under the auspices of the U.S. Department of Energy.

APPENDIX: LANCZOS METHOD

The generalized eigenvalue problem which we must solve in ρ,θ coordinates in Sec. III is of the form

$$Aa = \lambda Ba \,, \tag{A1}$$

where A and B are nonsymmetric real matrices. The eigenvector a contains the expansion coefficients a^{α}_{mn} of the reduced wave function

$$F_{\alpha} = \sum_{m=1}^{M} \sum_{n=1}^{N} a^{\alpha}_{mn} s_m(\rho) s_n(\theta) \,. \tag{A2}$$

The dimensionality of A and B for a calculation truncated at N_c channels is $N_c \times M \times N$, which even for modern supercomputers is too large to solve directly when N_c approaches 10. Because the two-body force on the left-hand side of Eq. (7) couples at most two channels, A is block diagonal. The dimensionality of these block diagonal terms is at most $2 \times M \times N$ ($M,N \simeq 30$ for the majority of our calculations), and matrix equations of the form

$$Aa = z \tag{A3}$$

can be solved efficiently one block at a time.

Because we seek the eigenvalues λ closest to unity, we consider the related equation

$$A^{-1}Ba = \frac{1}{\lambda} a \tag{A4}$$

or

$$Ha = \frac{1}{\lambda} a \,, \tag{A5}$$

such that $\lambda \simeq 1$ becomes one of the large eigenvalues. Note that $H = A^{-1}B$ is a nonsymmetric matrix.

To solve Eq. (A5), we use the Lanczos algorithm[27,28] to generate a small basis set which can be solved via standard eigenvalue programs. Assume an initial vector a_1 and generate the basis set a_i as well as the biorthogonal basis set b_i for $i = 1,2,\ldots,\nu$.

First, choose $b_1 \equiv a_1$ with $b_1^T a_1 = 1$. Second, generate

$$\tilde{a}_2 = Ha_1 - \alpha_1 a_1 \tag{A6a}$$

and

$$\tilde{b}_2 = H^T b_1 - \alpha_1 b_1 \,, \tag{A6b}$$

where α_1 is determined in such a manner that $\tilde{b}_2$ is orthogonal to a_1. That is, we choose

$$\alpha_1 = b_1^T H a_1 \,. \tag{A7}$$

The solutions of Eq. (A6) are obtained in two steps. We first find

$$c_1 = Ha_1 \tag{A8a}$$

and

$$d_1 = H^T b_1 \,. \tag{A8b}$$

To find c_1 we convert Eq. (A8a) to the form

$$Ac_1 = Ba_1 \tag{A9a}$$

or

$$Ac_1 = z \,. \tag{A9b}$$

Equation (A9b) can be solved one block at a time. To solve Eq. (A8b) we rewrite it in the form

$$d_1 = B^T (A^T)^{-1} b_1 \,. \tag{A10}$$

Then, if we define

$$e_1 = (A^T)^{-1} b_1 \tag{A11}$$

and solve the related equation

$$A^T e_1 = b_1 \tag{A12}$$

for e_1, we can obtain d_1 as

$$d_1 = B^T e_1 \ . \tag{A13}$$

Our Eqs. (A6) now have the form

$$\tilde{a}_2 = c_1 - \alpha_1 a_1 \tag{A6a'}$$

and

$$\tilde{b}_2 = d_1 - \alpha_1 b_1 \ , \tag{A6b'}$$

where α_1 is given by

$$\alpha_1 = b_1^T c_1 \ . \tag{A7'}$$

The normalization condition $b_2^T a_2 = 1$ is imposed following Saad.[28] We choose

$$a_2 = \tilde{a}_2 / | \tilde{b}_2^T \tilde{a}_2 |^{1/2} \tag{A14a}$$

and

$$b_2 = \tilde{b}_2 | \tilde{b}_2^T \tilde{a}_2 |^{1/2} / (\tilde{b}_2^T \tilde{a}_2) \ . \tag{A14b}$$

Given the first two vectors, we can generate the remaining vectors by means of the recursion relations

$$\tilde{a}_{i+1} = H a_i - \alpha_i a_i - \beta_i a_{i-1} \tag{A15a}$$

and

$$\tilde{b}_{i+1} = H^T b_i - \alpha_i b_i - \gamma_i b_{i-1} \ , \tag{A15b}$$

where

$$\alpha_i = b_i^T H a_i \tag{A16}$$

and

$$\gamma_i = | \tilde{b}_i^T \tilde{a}_i |^{1/2} \ , \tag{A17a}$$

$$\beta_i = \tilde{b}_i^T \tilde{a}_i / \gamma_i \tag{A17b}$$

are the normalization factors that determine $a_i = \tilde{a}_i / \gamma_i$ and $b_i = \tilde{b}_i / \beta_i$. Equations (A15) are solved using the same procedure that is followed to obtain $\tilde{a}_2$ and $\tilde{b}_2$.

Thus one can generate ν vectors a_i and their biorthogonal vectors b_i such that

$$b_i^T a_j = \delta_{ij} \ . \tag{A18}$$

Using this reduced basis set ($\nu \ll N_c \times M \times N$), we can write

$$a = \sum_{i=1}^{\nu} \epsilon_i a_i \ , \tag{A19}$$

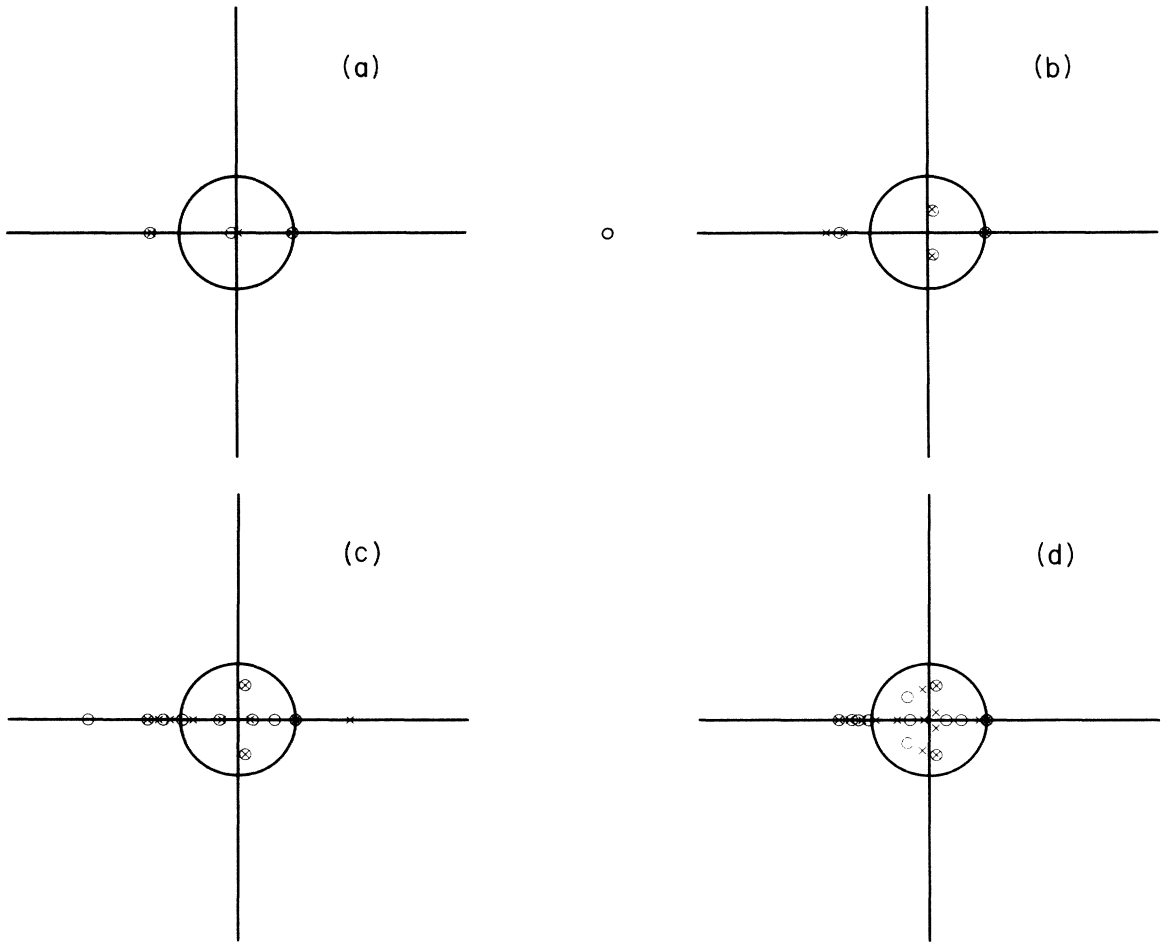

FIG. 3. Plots of $1/\lambda$ [Re$(1/\lambda)$ along the abscissa; Im$(1/\lambda)$ along the ordinate] for two different ρ, θ grids ($\circ$ and $\times$) as a function of the number of iterations ($\nu = 3,5,10,15$) for the Lanczos eigenvalue procedure discussed in the Appendix ($N_c = 3$).

and, after substituting this in Eq. (A5), we obtain

$$\sum_i \epsilon_i H a_i = \frac{1}{\lambda} \sum_i \epsilon_i a_i \ . \tag{A20}$$

The inner product with b_j^T leads to

$$\sum_i \epsilon_i b_j^T H a_i = \frac{1}{\lambda} \epsilon_j \ , \tag{A21}$$

or using Eq. (A15a)

$$\sum_i \epsilon_i (\gamma_{i+1}\delta_{i+1,j} + \alpha_i \delta_{ij} + \beta_i \delta_{i-1,j}) = \frac{1}{\lambda} \epsilon_j \ . \tag{A22}$$

Thus we are left to solve

$$\begin{bmatrix} \alpha_1 & \beta_2 & & & & \\ \gamma_2 & \alpha_2 & \beta_3 & & & \\ & \gamma_3 & \alpha_3 & \beta_4 & & \\ & & \cdot & \cdot & \cdot & \\ & & & \cdot & \cdot & \beta_n \\ & & & & \gamma_n & \alpha_n \end{bmatrix} \begin{bmatrix} \epsilon_1 \\ \epsilon_2 \\ \epsilon_3 \\ \cdot \\ \cdot \\ \epsilon_n \end{bmatrix} = \frac{1}{\lambda} \begin{bmatrix} \epsilon_1 \\ \epsilon_2 \\ \epsilon_3 \\ \cdot \\ \cdot \\ \epsilon_n \end{bmatrix} \ . \tag{A23}$$

The eigenvalues of this equation are approximations to the eigenvalues of our original matrix equation. In practice one increases ν until the change in λ is less than the desired accuracy. Normally 4 to 8 iterations is satisfactory. The expansion coefficients for the resulting approximation to the Faddeev amplitude are determined from Eq. (A19).

As an illustration of the results of the Lanczos method, we plot in Figs. 3(a)–(d) the eigenvalues $(1/\lambda)$ of Eq. (A22) in the complex plane (along with the unit circle) for two different ρ,θ grids (circles and crosses) as a function of the number of iterations $\nu=3$, 5, 10, and 15. Clearly, certain eigenvalues are manifestations of the mesh selected (circles and crosses not overlayed) while others are determined by the properties of the Hamiltonians, as they depend only upon the number of iterations. As the number of iterations is increased, the eigenvalues approach their limits; the largest eigenvalues converge the fastest. Actual eigenvalues of the Hamiltonian are those which are stable with respect to the number of iterations. Positive eigenvalues along the horizontal axis denote poles of the Hamiltonian for $1/\lambda$ times the given potential. Negative real eigenvalues correspond to bound-state poles for $-1/\lambda$ times the potential. For the power method to succeed, $\lambda=1$ must be the largest eigenvalue. The fact that some eigenvalues lie outside the unit circle implies that the power method would fail if applied directly to this Hamiltonian. The RSC NN potential yields one such eigenvalue; it must be removed before the power method will converge to the desired $\lambda=1$ solution. The 2π-3N force has much more structure at small distances and leads to several additional eigenvalues of that type, as can be seen in the plots. There are fewer eigenvalues than iterations for $\nu>10$, because some eigenvalues correspond to numerical noise and are too large to appear on the plot.

*Present address: Department of Physics and Astronomy, University of Rochester, Rochester, NY 14627.

[1]J. L. Friar, B. F. Gibson, and G. L. Payne, Annu. Rev. Nucl. Sci. **34**, 403 (1984).

[2]See, for example, J. L. Friar, Nucl. Phys. **A353**, 233c (1981) for a discussion of the first two categories.

[3]I. Sick, *Lecture Notes in Physics* (Springer, Berlin, 1978), Vol. 87, p. 236.

[4]J. Torre, J. J. Benayoun, and J. Chauvin, Z. Phys. A **300**, 319 (1981).

[5]Muslim, Y. E. Kim, and T. Ueda, Phys. Lett. **115B**, 273 (1982); Nucl. Phys. **A393**, 399 (1983).

[6]W. Glöckle, Nucl. Phys. **A381**, 343 (1982); A. Bömelburg, Phys. Rev. C **28**, 403 (1983); A. Bömelburg and W. Glöckle, *ibid.* **28**, 2149 (1983).

[7]J. Carlson, V. R. Pandharipande, and R. B. Wiringa, Nucl. Phys. **A401**, 59 (1983); R. B. Wiringa, *ibid.* **A401**, 86 (1983).

[8]R. B. Wiringa, J. L. Friar, B. F. Gibson, G. L. Payne, and C. R. Chen, Phys. Lett. **143B**, 273 (1984).

[9]S. Ishikawa, T. Sasakawa, T. Sawada, and T. Ueda, Phys. Rev. Lett. **53**, 1877 (1984).

[10]S. A. Coon, M. D. Scadron, P. C. McNamee, B. R. Barrett, D. W. E. Blatt, and B. H. J. McKellar, Nucl. Phys. **A317**, 242 (1979); S. A. Coon and W. Glöckle, Phys. Rev. C **23**, 1790 (1981).

[11]H. T. Coelho, T. K. Das, and M. R. Robilotta, Phys. Rev. C **28**, 1812 (1983).

[12]J. I. Fujita and H. Miyazawa, Prog. Theor. Phys. **17**, 360 (1957).

[13]C. Hadjuk and P. U. Sauer, Nucl. Phys. **A322**, 329 (1979); C. Hadjuk, P. U. Sauer, and W. Strueve, *ibid.* **A405**, 581 (1983); P. U. Sauer, Nuovo Cimento **76**, 309 (1983).

[14]C. R. Chen, G. L. Payne, J. L. Friar, and B. F. Gibson, Phys. Rev. Lett. **55**, 374 (1985).

[15]J. Carlson, V. R. Pandharipande, and R. B. Wiringa, Nucl. Phys. **A401**, 59 (1983); R. Schiavilla, V. R. Panharipande, and R. B. Wiringa, *ibid.* **A449**, 219 (1986).

[16]R. V. Reid, Ann. Phys. (N.Y.) **50**, 411 (1968); B. Day, Phys. Rev. C **24**, 1203 (1981).

[17]R. B. Wiringa, R. A. Smith, and T. A. Ainsworth, Phys. Rev. C **29**, 1207 (1984).

[18]C. R. Chen, G. L. Payne, J. L. Friar, and B. F. Gibson, Phys. Rev. C **31**, 2266 (1985).

[19]C. R. Chen, Ph.D. dissertation, University of Iowa, 1985.

[20]G. L. Payne, J. L. Friar, B. F. Gibson, and I. R. Afnan, Phys. Rev. C **22**, 823 (1980).

[21]L. D. Faddeev, Zh. Eksp. Teor. Fiz. **39**, 1459 (1960) [Sov. Phys.—JETP 12, 1014 (1961)].

[22]H. P. Noyes, in *Three Body Problems in Nuclear and Particle Physics,* edited by J. S. C. McKee and P. M. Rolph (North-Holland, Amsterdam, 1970), p. 2.

[23]E. P. Harper, Y. E. Kim, and A. Tubis, Phys. Rev. C **2**, 877 (1970); **6**, 126 (1972).

[24]E. L. Slaggie and E. H. Wichman, J. Math. Phys. **3**, 946 (1962).

[25]P. M. Prenter, *Splines and Variational Methods* (Wiley, New York, 1975).

[26]C. R. Chen, G. L. Payne, J. L. Friar, and B. F. Gibson, Phys.

Rev. C **31**, 2266 (1985).
[27]C. Lanczos, J. Res. Nat. Bur. Stand. **49**, 33 (1952).
[28]Y. Saad, SIAM (Soc. Ind. Appl. Math.) J. Num. Anal. **19**, 485 (1982).
[29]J. L. Friar, B. F. Gibson, and G. L. Payne, Phys. Rev. C **24**, 2279 (1981).
[30]C. Hajduk, private communication.
[31]R. G. Ellis, S. A. Coon, and B. H. J. McKellar, Nucl. Phys. **A438**, 631 (1985).
[32]S. A. Coon and M. D. Scadron, Phys. Rev. C **23**, 1150 (1981).
[33]G. L. Payne, J. L. Friar, and B. F. Gibson, Phys. Rev. C **22**, 832 (1980).
[34]B. Frois, private communication; note that these data differ from those on similar plots in Ref. 35.
[35]J. L. Friar, B. F. Gibson, C. R. Chen, and G. L. Payne, Phys. Lett. **161B**, 241 (1985).
[36]R. B. Wiringa, private communication.
[37]T. Sasakawa and S. Ishikawa, Few-body Systems **1**, 3 (1986).